Biomechanics and Modeling in Mechanobiology accepted manuscript. Published version is available at:
https://doi.org/10.1007/s10237-020-01293-9

An adaptive-remeshing framework to predict impact-induced skull fracture in infants

Junyan He[1], **Jiawei Yan**[1],
Susan Margulies[2], **Brittany Coats**[1], **Ashley D. Spear**[1*]

Received: Septemeber 24, 2019 / Accepted: January 14, 2020

Abstract Infant skull fractures are common in both accidental and abusive head trauma, but identifying the cause of injury may be challenging without adequate evidence. To better understand the mechanics of infant skull fracture and identify environmental variables that lead to certain skull fracture patterns, we developed a computational framework that utilizes linear elastic fracture mechanics theory to predict skull fracture. The finite element method and adaptive remeshing technique were employed to simulate high-fidelity, geometrically explicit crack propagation in an infant skull following impact. In the framework, three modes of stress intensity factors are calculated by means of the M-integral using the commercial analysis code, FRANC3D, and are used as measures of crack driving force. The anisotropy of infant skulls is represented by means of a transversely isotropic constitutive model and a direction-dependent fracture toughness locus. The ability of the framework to predict impact-induced fracture patterns is validated by comparison with experimentally observed fracture patterns from the literature.

Keywords Computational fracture mechanics, Infant skull fracture, Crack growth, Linear elastic fracture mechanics

[1] Department of Mechanical Engineering, University of Utah, Salt Lake City, Utah, USA

[2] Department of Biomedical Engineering, Georgia Institute of Technology, Atlanta, Georgia, USA

* Corresponding author
Tel.: (801) 581-4753
E-mail: ashley.spear@utah.edu

1 Introduction

In 2017, approximately 3.5 million children in the U.S. were victims of child maltreatment and abuse (U.S. Department of Health & Human Services, Administration for Children and Families, Administration on Children, Youth and Families, Childrens Bureau 2019). Under current Department of Justice guidelines, an important indicator of physical abuse is the inability of the caretaker to provide a history that corresponds to the observed injuries of the child (Farley et al. 2002). When no history of trauma is presented, identifying discrepancies to injuries may be straight forward. However, when a history of a fall is provided, distinguishing between abusive and accidental trauma may prove to be challenging, especially if the injuries are limited to skull fracture and underlying head trauma. Skull fractures are common in both accidental and abusive head trauma (Leventhal et al. 1993), but very little is known about the mechanics of skull fractures from accidental fall in infants. The ability to objectively identify the cause of skull fracture and understand the sensitivity of skull fracture patterns to impact conditions (i.e. direction, height, surface conditions) can substantially improve the accurate detection of child abuse.

Previous experimental research efforts have focused on exploring the impact response of the infant head and the connections between types of loading and the resulting skull fracture patterns (Hodgson et al. 1970; Got et al. 1978; Weber 1984, 1985; Loyd 2011). In these studies, cadavers were dropped from various heights onto various surfaces. Unfortunately, detailed quantitative descriptions of the impact conditions are lacking in many of the studies. In a more recent study, Loyd (2011) studied the force and acceleration curves from infant cadaver head drop experiments and reported skull fracture patterns. More information is provided on the head orientation prior to each drop, but the exact im-

pact location and impact angle was not measured. These limitations make computational modeling challenging, but the studies still provide valuable data to qualitatively validate skull fracture predictions.

Realizing the lack of sufficient human specimens to perform comprehensive tests, researchers have explored pediatric head injury from a computational perspective. Finite element (FE) models have been constructed from computed tomography (CT) scans and used to simulate the stress and strain response of the human infant skull during impact (Li et al. 2013, 2015). Comparing the stress/strain fields from FE simulations and the observed fracture patterns, researchers have formulated crack initiation criteria that identify potential initiation sites for cracks (Coats et al. 2007; Coats 2007; Roth et al. 2008; Hajiaghamemar et al. 2018). These studies use high-strain-rate material property data from infant skull specimens (Coats and Margulies 2006), but none of the above-mentioned works explore how cracks propagate under the given loads. More recent studies investigated crack propagation in infant skulls using an element deletion method (Zhang et al. 2001; Lee et al. 2009; Sahoo et al. 2013; Asgharpour et al. 2014). Element deletion is a commonly used method because it requires minimal modification to the standard FE procedure. In this method, a damage variable is calculated based on a damage criterion, and stress is scaled down based on this damage variable. When an element fails, its stress is reduced to zero. By sequential failure of elements, a "crack"can be formed and propagated. Since elements of the mesh are deleted, the final fracture patterns depend on the initial mesh. Furthermore, no crack geometry is included in this method, therefore the singular stress/strain fields near the crack tip that dictate the crack path are not captured. In other words, the deletion of elements simply leads to the appearance of a fracture surface, but fracture is technically not simulated. Other computational methods like the extended finite element method (Song et al. 2006) and adaptive remeshing (Davis et al. 2014) have been used to study crack propagation in complex geometries. However, the application of such methods have been mostly focused on analyzing engineering components and structures, not biological structures. The area of studying crack propagation on biomaterials using well-established computational fracture mechanics methods remains largely unexplored.

The objective of this work was to develop a computational framework that can assist in the differential diagnosis between accidental and abusive head trauma by enabling high-fidelity simulation of crack propagation in infant skulls using principles of linear elastic fracture mechanics (LEFM). To achieve this objective, we selected an adaptive remeshing technique to predict crack propagation. In this method, the crack face is first represented as a virtual boundary in the geometry. Every time the crack propagates, the mesh is updated and the element edges and faces are forced to conform to this virtual boundary. In this way, the crack face is represented explicitly in the resulting mesh by element edges and faces. To capture the high-gradient stress field, quarter-point elements can be used, which produce the desired singularity in the element shape functions (Shih et al. 1976; Lynn and Ingraffea 1978). Various examples of adaptive remeshing can be found in the literature (Wawrzynek et al. 2010; Chin 2011; Spear et al. 2011; Davis et al. 2014). The largest disadvantage of this method is the constant need to remesh. However, adaptive remeshing is more appropriate when dealing with crack-face contact (Corbani et al. 2018) as well as crack closure (Nguyen et al. 2001). In addition, since quarter-point elements are used near the crack tip, a relatively coarse mesh can still provide an accurate characterization of the stress field. Finally, among all of the available FE-based approaches, adaptive remeshing can conform to complex, three-dimensional crack surfaces as predicted by fracture mechanics, thus resulting in minimal mesh dependency. Once developed, this computational framework will be invaluable to the investigation of skull fracture patterns in infants from accidental and abusive head trauma.

2 Framework Development

2.1 Overview of Framework

The overarching goal of this framework is to simulate crack propagation in an infant skull FE model. To do so, we start by inspecting the stress/strain distribution throughout an uncracked model during a simulated impact event to identify potential locations of crack initiation, similar to our previous work (Coats et al. 2007; Hajiaghamemar et al. 2018). Once the location of crack initiation is determined, we identify the preferred crack orientation by comparing stress intensity factors (SIFs) for cracks inserted at the same location but with different orientations. When both the location and orientation are determined, we employ the commercial software FRANC3D (Wawrzynek et al. 2010) to insert the initial crack. We discretize the crack growth process into crack-growth time steps. In each time step, SIFs are computed and used to determine if the crack will propagate, and if so, in what direction. Every time a crack is propagated, crack stability is checked and the crack is propagated in the same time step if it is unstable. A high-level flowchart of the simulation framework is provided in Figure 1. The following subsections describe each step in detail.

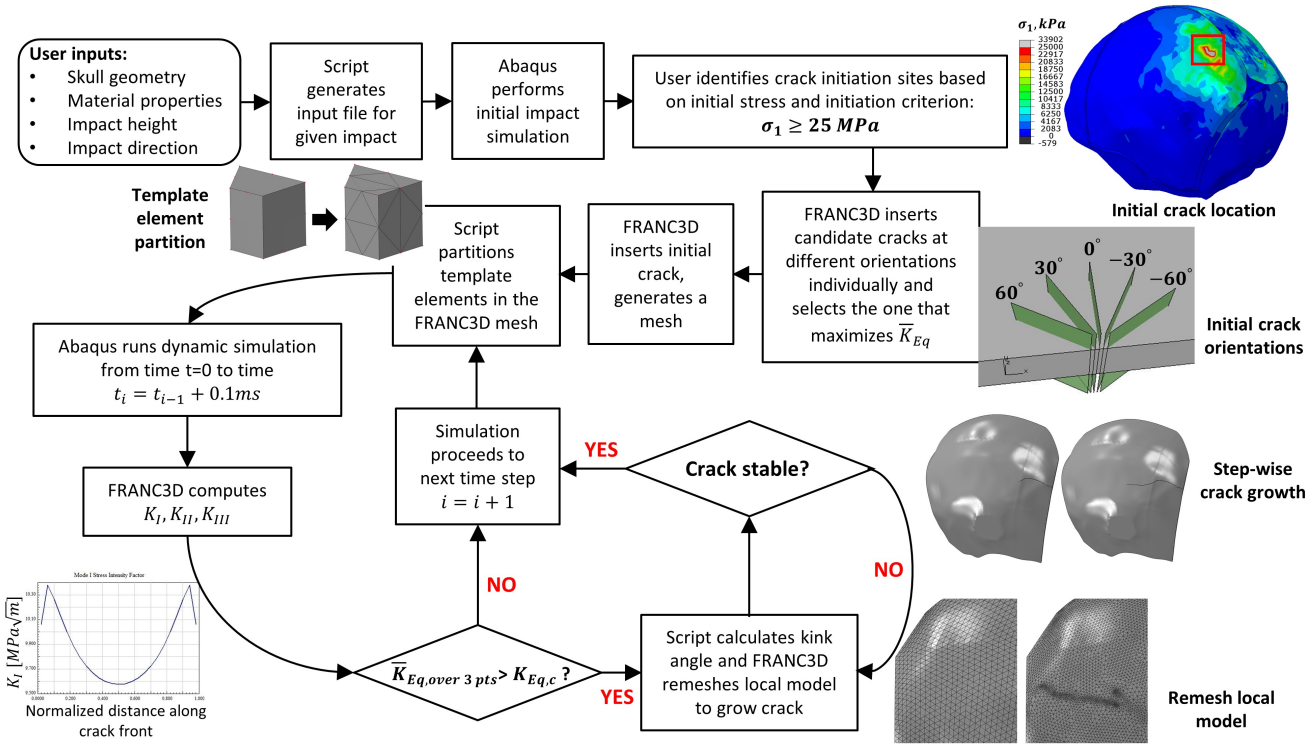

Fig. 1 Adaptive remeshing framework for simulating crack growth during an explicit dynamic simulation.

2.2 Model Definitions

An impact case is uniquely defined by the skull geometry, material properties, impact direction, and impact height. The skull FE model used in this work is adopted from the work by Coats et al. (2007). The material properties used in the model are presented in Table 1, and are adopted from works by Metcalf et al. (2019) as well as Coats and Margulies (2006).

Table 1 Material properties of the infant skull FE model in this work

Region	E_1 (MPa)	E_2 (MPa)	E_3 (MPa)	ν_{12}	ν_{23}
Parietal	468	453	453	0.28	0.465
Occipital	402	300	300	0.28	0.465
Rest of skull	407	407	407	0.19	0.19
Suture	8.1	8.1	8.1	0.49	0.49

The direction of impact is defined as a vector, using a spherical coordinate system centered at the skull's center of mass. Figure 2 illustrates this coordinate system. The azimuthal angle, ϕ, and the polar angle, θ, are provided by the user, which together define a unit direction vector. The impact velocity vector is parallel to the impact direction vector. A rigid plate (the impact surface) in the model is then translated and rotated such that it is perpendicular to the velocity vector (i.e. creates a normal impact). The magnitude of the initial velocity immediately before impact is calculated from impact height H using:

$$V_{initial} = \sqrt{2gH}, \tag{1}$$

where g in the local gravitational acceleration.

The Cartesian components of velocity in the Abaqus global coordinate system are computed from the components of the impact direction vector. From here on, an impact case will be referred to as an array of parameters: [ϕ, θ, H]. After all impact parameters are determined, an Abaqus input file is generated. Using this input file, a dynamic simulation of the uncracked model is conducted to extract stress/strain response.

2.3 Initial Crack Insertion

Based on the criterion proposed by Hajiaghamemar et al. (2018), a crack on human skulls tends to initiate in the location where the maximum principal stress first exceeds 25 MPa, with a 50% probability. In this work, we adopted the same criteria. The framework inserts a crack at the location where the average maximum principal stress of an element first exceeds 25 MPa. The time instance where the criterion

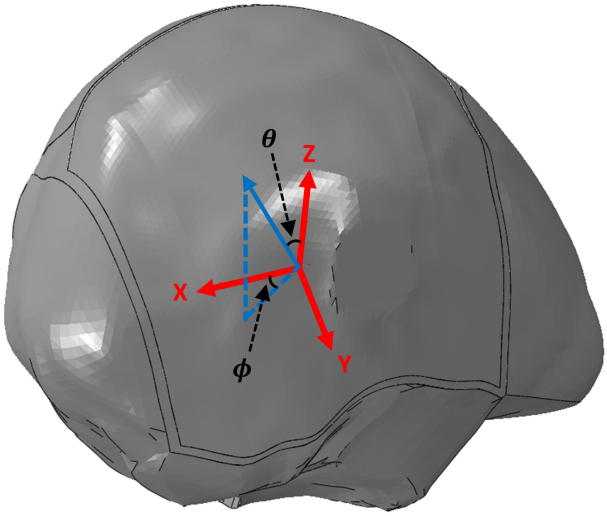

Fig. 2 Definition of the impact direction vector (blue arrow) using two angles (ϕ and θ) in the local coordinate system.

is first exceeded is denoted as $t_{initial}$.

In this framework, we assumed that any initial crack will be oriented such that the equivalent stress intensity factor (K_{Eq}) is maximized. The equivalent stress intensity factor is defined as:

$$K_{Eq} = \sqrt{K_I^2 + K_{II}^2 + K_{III}^2}, \tag{2}$$

where K_I, K_{II} and K_{III} denote the Mode I, II and III stress intensity factors, respectively.

To determine the initial crack orientation, a single crack of length 2 mm is inserted in the model at five different orientations ($\pm 60°$, $\pm 30°$and $0°$) in five independent simulations. An initial crack length of 2 mm was chosen as the initial crack length to match the resolution of clinical CT scanners commonly used to identify fractures in bones (Vannier et al. 1984; Jacobsen et al. 2009; Grassberger et al. 2011). Displacements, stresses, and crack-face contact forces at time $t = t_{initial}$ are extracted to compute all three modes of SIFs for each crack orientation. The orientation that yields the highest average K_{Eq} value along the crack front is considered to be the mechanically preferred orientation of the initial crack. Figure 3 depicts the process of identifying the location of initial crack and the orientations of candidate cracks considered in the framework. Even though Figure 3 only shows one initiation site, multiple initiation sites at different locations are possible provided that they meet the initiation criterion. The same procedure is applied to each initiation site to determine its preferred orientation.

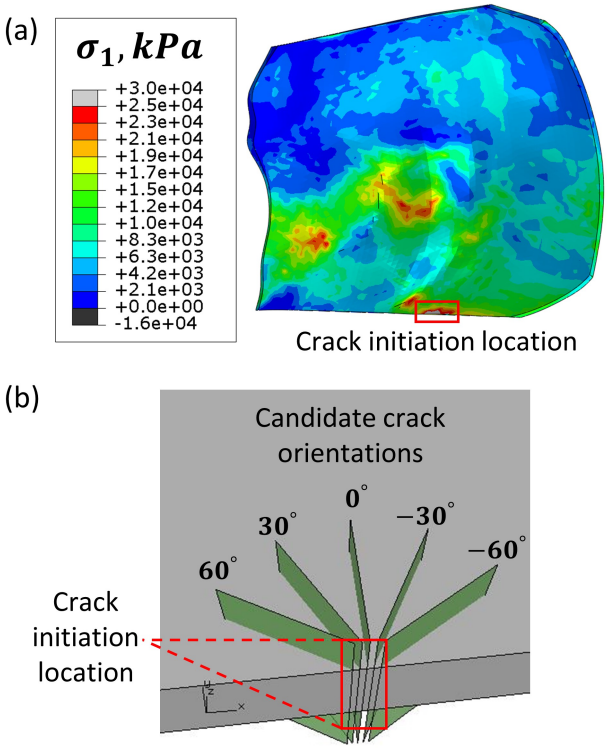

Fig. 3 (a) Example maximum principal stress distribution on the right parietal bone with the crack initiation site identified (box). The rest of the skull is hidden for visualization. (b) Five possible crack orientations inserted on the same model for visualization.

2.4 Stress Intensity Factors Calculation

In this work, continuous crack growth during impact is approximated by discrete time steps, each of duration 0.1 ms. In time step i, the duration of the impact simulation is $t_{current} = t_{initial} + i * 0.1$ms. SIFs are calculated in each time step for all crack fronts as the crack growth driving force.

In FRANC3D, the M-integral (Yau et al. 1980) is the most accurate method for extracting SIFs (Fracture Analysis Consultants, Inc 2018). However, structured, quadratic template elements (e.g. quadratic wedge, C3D15, and quadratic hexahedron, C3D20) are needed on the crack front to allow for calculation of M-integral in the FRANC3D implementation (v.7.1.1). The above-mentioned element types are not supported in Abaqus/Explicit (v.6.16) element library. To allow for calculation of the M-integral in explicit simulations, an in-house code was built into the framework to modify the mesh prior to the analysis. In this step, each unsupported element is partitioned into multiple linear tetrahedral (i.e. C3D4) elements, while preserving all nodes of the original quadratic element. Figure 4 illustrates this partition process on two element types. The effect of partitioning on the accuracy of SIFs was assessed by a case study, whose results are presented in Table 2. Partitioning inevitably introduces error, due to reduction of element quality and loss of quadratic

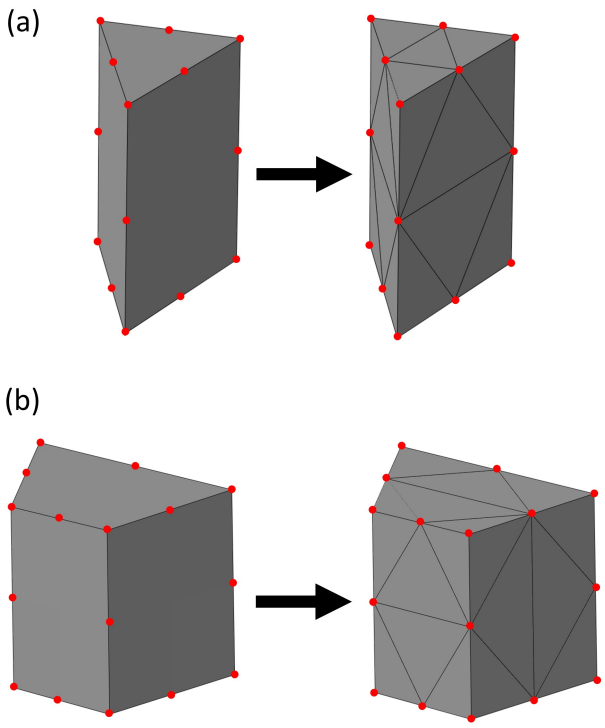

Fig. 4 Partition process on (a) C3D15 (b) C3D20 (nodes shown with red dots) Note that all nodes are retained before and after partition.

Table 2 Comparison of averaged SIFs from two methods

Mode	Quadratic template elements (MPa$\sqrt{mm}$)	Partitioned linear elements (MPa$\sqrt{mm}$)	Percent difference
K_I	10240.39	11017.31	7.62%
K_{II}	-18963.32	-20227.73	6.72%
K_{III}	-7255.44	-7144.19	-0.23%

shape functions. The maximum error induced by partitioning was 7.62%, with a mean error of 4.7%, which was considered acceptable for our framework.

Once the partition process is completed, Abaqus/Explicit is used to analyze the modified mesh. FRANC3D leverages displacements and contact forces on the crack-front template nodes to compute SIFs.

2.5 Crack Propagation

Crack propagation is dictated by a material's resistance to crack growth (i.e., the material fracture toughness). In bones, crack toughening mechanisms (i.e. crack bridging) lead to an increased fracture toughness with increased crack length (Nalla et al. 2005; Zimmermann et al. 2010). Such behavior is modeled by an increasing R curve. In the absence of experimental data for human infant cranial bone, the R curve was assumed to take an exponential form. This hypothetical relation is given in Equation 3:

$$K_{Ic}(a) = K_{Ic,0}(2 - e^{-0.05a}), \tag{3}$$

where $K_{Ic,0}$ and a denote the initial Mode I fracture toughness and the crack length, respectively.

In human cortical bones, crack-growth resistance depends not only on crack length, but also on collagen fiber direction (Nalla et al. 2005; Koester et al. 2008). Since infant skulls contain trabecular fibers that radiate outward from the ossification center, it is reasonable to assume that skull fracture toughness also depends on fiber direction. Pettit (2000) proposed the following empirical relationship that relates fracture toughness in any arbitrary direction to the two principal fracture-toughness values:

$$K_{Ic}(\beta) = K_{Ic,\parallel} cos^2\beta + K_{Ic,\perp} sin^2\beta, \tag{4}$$

where β is the angle between an infinitesimal crack extension and local fiber direction. $K_{Ic,\parallel}$ and $K_{Ic,\perp}$ denote the Mode I fracture toughness parallel and perpendicular to fiber direction, respectively.

For convenience, let:

$$\frac{K_{Ic,\perp}}{K_{Ic,\parallel}} = \lambda. \tag{5}$$

In the proof-of-concept simulations presented in Section 3, λ was assumed to be 10 in all simulations. This value is comparable to that observed in human cortical bone specimens by Koester et al. (2008).

Combining Equations (3), (4) and (5), we have an expression of the evolution of fracture toughness, or, the R curve:

$$K_{Ic}(\beta, a) = K_{Ic,\parallel,0}(2 - e^{-0.05a})(cos^2\beta + \lambda sin^2\beta). \tag{6}$$

From data reported by Bojtár et al. (1994), Mode I fracture toughness of human adult skull is approximately 23.7±6.99 MPa$\sqrt{\text{mm}}$. It is reasonable to assume that infant skulls have lower strength than adult ones. Due to the lack of experimental data on infant skulls, $K_{Ic,\parallel,0}$ was assumed to be 5 MPa$\sqrt{\text{mm}}$, which is about 21% of that of adult skull.

In this work, the maximum generalized stress criterion (Fracture Analysis Consultants, Inc 2018) was adopted to calculate crack kink angle, which is a combination of the

maximum tangential stress criterion (Erdogan and Sih 1963) and the maximum shear stress criterion. For an isotropic material, SIFs of an infinitesimal crack extension at angle $\Delta\alpha$, denoted by k, can be related to SIFs of the main crack as (Pettit et al. 2013):

$$k_I(\Delta\alpha) = cos\frac{\Delta\alpha}{2}(K_I cos^2\frac{\Delta\alpha}{2} - \frac{3}{2}K_{II}sin\Delta\alpha), \quad (7)$$

$$k_{II}(\Delta\alpha) = \frac{1}{2}cos\frac{\Delta\alpha}{2}(K_I sin\Delta\alpha + K_{II}(3cos\Delta\alpha - 1)), \quad (8)$$

$$k_{III}(\Delta\alpha) = K_{III}cos\frac{\Delta\alpha}{2}. \quad (9)$$

Even though infant skull bones are highly anisotropic, we assume that the above relationships hold. The maximum generalized stress criterion predicts that crack kinks at an angle $\Delta\alpha$ that maximizes the driving force (either opening or shearing). The maximum driving force is defined as:

$$k_{max}(\Delta\alpha) = max[k_I(\Delta\alpha), k_s(\Delta\alpha)], \quad (10)$$

where $k_s(\Delta\alpha)$ is defined as :

$$k_s(\Delta\alpha) = \sqrt{[c_2 k_{II}(\Delta\alpha)]^2 + [c_3 k_{III}(\Delta\alpha)]^2}. \quad (11)$$

The coefficients c_2 and c_3 in Equation (11) are user-defined weight factors to tune the contribution of Mode II shearing and Mode III tearing to better match experimental kink-angle observations (Fracture Analysis Consultants, Inc 2018).

At the onset of crack propagation, LEFM requires that the local driving force exceeds the local fracture toughness. That is:

$$\begin{aligned} &k_{max}(\Delta\alpha) \geq K_{Ic}(\beta, a), \text{ if } k_{max}(\Delta\alpha) = k_I(\Delta\alpha), \\ &k_{max}(\Delta\alpha) \geq 0.866K_{Ic}(\beta, a), \text{ if } k_{max}(\Delta\alpha) = k_s(\Delta\alpha). \end{aligned} \quad (12)$$

When driving force is dominated by shear (i.e. $k_{max}(\Delta\alpha) = k_s(\Delta\alpha)$), Erdogan and Sih (1963) proposed in the maximum tangential stress criterion that K_{IIc} can be estimated as $0.866K_{Ic}$, hence the scaling factor in Equation (12). The kink angle $\Delta\alpha$ can now be found by numerically maximizing Equation (10) while satisfying the inequality in Equation (12). When the kink angle is found, the crack is advanced in this direction by a uniform amount of 2 mm. Again, this crack extension is selected to be comparable to the resolution of common clinical CT scanners. FRANC3D reads the crack propagation information (viz., new crack front coordinates) and remeshes the model to reflect the new crack geometry. In cases when inequality (12) is not satisfied for any admissible $\Delta\alpha$ between -90°and 90°, no crack growth will occur in the current load step and the same crack geometry is used in the next analysis step.

2.6 Crack Stability

Whenever a crack propagates, crack stability is checked before moving to the next time increment. To do so, the newly formed crack is loaded again to the current time increment, where SIFs are evaluated on the new crack front. If inequality (12) is again satisfied (i.e. crack is predicted to propagate without any increase in load), this crack is considered to be unstable and will be propagated again in the current time increment. This check process is repeated until the crack stops growing in the current time increment. Then, the analysis proceeds to the next time increment where steps described in sections 2.4 through 2.6 are repeated until the end of total impact duration. Crack growth is said to be complete either when the end of total impact duration is reached or when the crack extends through the parietal bone of the skull.

2.7 Proof-of-Concept Simulations

To evaluate the predictability of the framework, three proof-of-concept simulations were performed. In the first proof-of-concept simulation, we simulated a 14.7 cm drop test of a 5-month-old infant head specimen as described by Loyd (2011). No information on impact angles was provided. Using trial-and-error, we found that parameter set [30°,0°,14.7 cm] gives a crack-initiation location similar to that observed in the experiment. The mass of the model was scaled uniformly to match that reported by Loyd.

In the second and third proof-of-concept simulation simulated two 82 cm drop experiments reported by Weber (1984) using one 2.3-month-old (case A1) and one 4-month-old (case A3) infant whole body specimens, respectively. The mass of the model was scaled to match that reported in each experiment. Similar to Loyd, no impact angles data were provided. Again by trial-and-error, we found that parameter sets [-50°,0°,82 cm] and [-40°,-50°,82 cm] gave reasonable initiation locations for cases A1 and A3, respectively, based on the hand-drawn figures of fracture patterns provided.

3 Results

3.1 Comparison with Loyd 2011 Data

For the first simulation, at an impact height of 14.7 cm, the maximum principal stress did not exceed our threshold of 25 MPa. Since fracture was observed in the experiment, we lowered our stress threshold to 12 MPa for this simulation, which is approximately the 15th percentile of the parietal ultimate stress distribution, according to data reported by Coats (2007). Given the natural variability in

the pediatric skull and other factors that could effect fracture initiation (i.e., cadaver handling, freeze/thawing, etc), we consider this decrease realistic. This threshold was first exceeded at t=0.0026 s on the anterior edge of the right parietal bone. Starting from this time increment, a total of 60 time steps were simulated using the simulation framework described in Figure 1. The crack grew 17 times, reaching a final crack length of approximately 37 mm (measured by tracing each crack increment along the mesh outer surface). The crack extended nominally along the direction of trabecular fibers and eventually arrested near the ossification center. The overall kink angle, as measured from the end of the crack to the coronal suture line is 82.6°. Loyd observed a similar linear fracture nominally along the fiber direction with a reported length of 40 mm and overall kink angle of about 83.18°(measured by our group from the projection drawing). The comparison between the simulated result and Loyd's experimental result is presented in Figure 5. The figure from Loyd's paper is modified to only show the right parietal bone region. The simulated result shows good agreement with the experiment in terms of both crack length and nominal crack angle.

3.2 Comparison with Weber 1984 Data

For simulation of case A1, an edge crack initiated on the posterior edge of the right parietal bone. It curved slightly and continued to extend nominally along direction of the trabecular fibers, see Figure 6 (c). In Weber's study, the crack curved as it extended away from the posterior edge, similar to our simulation prediction, but at a much more pronounced angle. The experimentally observed crack from Weber covered about 80% of the right parietal bone length. Thus was longer than the simulation prediction, which covered about 70% of the right parietal bone length. A small crack branching was observed in the experiment, but the current framework does not allow for the representation of a branched crack so it was not captured in the simulation.

For simulation of case A3, two crack initiation sites were predicted by the framework, see Figure 6 (d). One of the cracks initiated on the posterior edge of the right parietal bone and the other initiated near the ossification center. The two cracks came close to coalescing but were manually arrested since crack coalescence is not possible in the current framework. The two cracks remain nominally parallel to the superior edge of the right parietal bone until the center crack approached the anterior edge of the right parietal bone, where it extended downward to the anterior inferior corner of the bone. Two nearly coalescing cracks were observed in the experimental drawing as well. However, in Weber's study, the center crack extended into the frontal bone. A small crack branching was observed for the center crack.

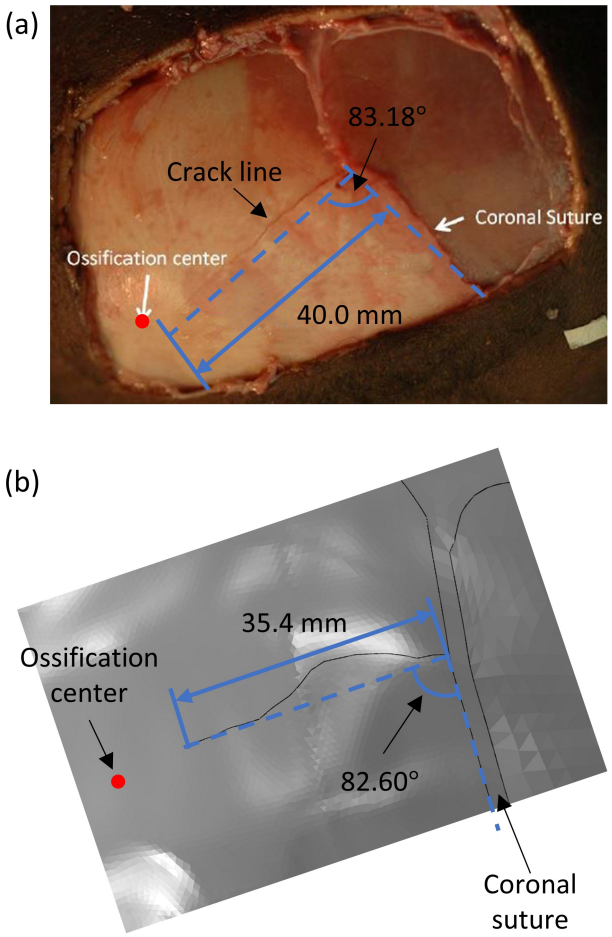

Fig. 5 Comparison with Loyd's experiment (a) Observed crack from experiment (Adapted by permission from Loyd (Loyd 2011)). The crack is mostly linear with a tip-to-tail length of 40 mm (b) Simulated result using the computational framework. The simulated crack has a tip-to-tail length of 35.4 mm and actual crack length of 37.0 mm.

Neither the extension into the frontal bone nor the crack branching were captured in the simulation as those features are not currently supported.

The strong similarities between the simulation and the experimental data illustrate the high potential for accurate, high-fidelity fracture pattern prediction using our framework, especially with the limited amount of data available to us in simulating the experiments. The similarity between simulation and experiment results would likely improve if the impact parameters and skull geometries are known accurately.

4 Discussion

In this work, we developed the first computational framework for predicting infant skull fracture based on linear elastic fracture mechanics using adaptive-remeshing technique.

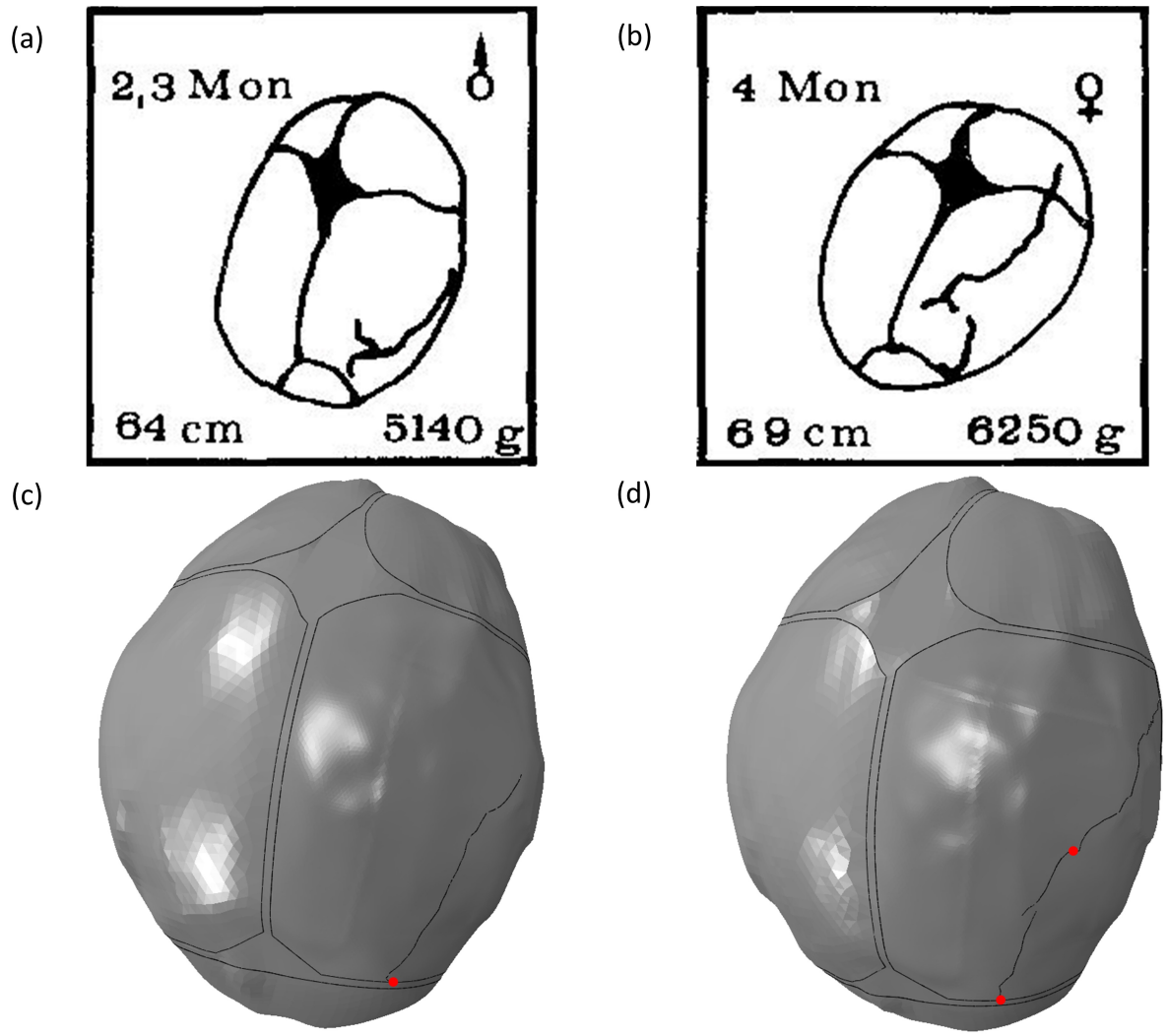

Fig. 6 Weber (1984) experimental results (adapted by permission from Springer Nature: Springer, Zeitschrift fur Rechtsmedizin) and simulated results. (a-b) Weber's cadaver experimental fracture patterns from a 82 cm drop of (a) case A1, a 2.3-month-old infant and (b) case A3, a 4-month-old infant onto concrete. (c-d) Associated fracture patterns predicted from the computational framework. Crack initiation sites are marked with red dots. In (c), the framework predicted similar crack length to (a), but did not capture the small branched crack. In (d), the framework predicted two separate cracks, which is in agreement with the Weber drawings in (b). However, the anterior crack terminated in the inferior region of the bone rather than crossing over the coronal suture.

Four aspects of this framework deserve further discussion: (1) framework performance as compared to previous works, (2) FE model and constitutive relations, (3) assumptions made in the framework and (4) potential applications.

Many previous works explored prediction of skull fracture via an element deletion method (Raul et al. 2006; Roth et al. 2010; Li et al. 2019). To obtain decent results using an element deletion method, the mesh size must be sufficiently small, since the element size dictates the resolution of crack propagation. In early work like that by Raul et al. (2006), the element size was relatively large (about 5 mm), possibly due to limited computational power available. This resulted in unrealistic patchy and disconnected fracture patterns. The element size was reduced in work by Roth et al. (2010), but the resulting fracture pattern was still zigzagged due to the hexahedral elements used in the model. Whereas in our framework, since element faces are arranged in the remeshing process to conform to the crack face, a smooth representation of the crack geometry can be guaranteed and the crack growth resolution is independent of element size. Nonetheless, when a very refined mesh is used, element deletion method can predict a smooth crack pattern (Li et al. 2019). However, in the work by Li et al. (2019), despite the smooth crack pattern, the framework only predicted some of the many crack initiation sites and had some variation from the experimental crack paths. In comparison, our framework predicted all crack initiation sites for the three

proof-of-concept simulations and all of them show similar nominal crack kink angle.

It is important to highlight that the implementation of the current framework is independent of the FE model and material properties. This framework can be coupled with a case-specific FE model and material properties to produce case-specific predictions, as opposed to using the same model for different cases. The framework also leaves freedom for the researcher to tune fracture parameters of the model (e.g. mixed-mode weight factors, R curve equation) to better match experimental observations. Although the maximum generalized stress criterion is used for calculating kink angle in the current framework, this choice is somewhat arbitrary. Some researchers suggest that the maximum tangential stress criterion better describes experimental results (Nalla et al. 2005; Hazenberg et al. 2006; Koester et al. 2008), while others suggest the use of the maximum strain energy release rate criterion (Zimmermann et al. 2010). However, there is not a definitive consensus on which one is better. Any of these kink angle models can be explored by the user without loss of generality.

Many assumptions and simplifications were employed in this framework. We set 2 mm as the length of the initial crack as well as the uniform extension increment of the crack front. Further, a crack was assumed to propagate along a single kink angle and with uniform extension along the three-dimensional crack front. Neither of these assumptions occur in real-life, but were necessary simplifications to balance accuracy, meshability, and computational efficiency. Non-uniform crack growth with individual kink angles for all crack front nodes is possible, but typically performed in simplified geometry. Creating a complex crack front in an already complex geometry, all while maintaining a structured crack-front template mesh (Warzynek et al. 2005) would be inherently challenging. Increasing complexity in these features may be explored in future iterations of the framework. It is also worth noting that the relationships in Equations (7)-(9) are for isotropic materials. They were assumed to hold even for the anisotropic skull in this work. It is unknown if this is a reasonable assumption. Future experimental efforts are needed to help elucidate the implications of this assumption.

Regardless of these assumptions, the three proof of concept simulations bore striking similarities to their experimental counterparts. The general paths and lengths of the fracture patterns were in agreement. Limitations of the framework prevented finer details such as crack branching, and we hope to explore solutions for these aspects in the future. However, in it's current state, the framework provides a reasonable approximation of the primary fracture pattern and will be extremely useful in parametric simulations investigating the effects of impact energy, directionality, and geometrical features on skull fracture in infants.

In summary, this framework provides a tool to study impact-induced fracture on infant skulls from a computational perspective. Using this framework, the sensitivity of impact conditions on resulting fracture patterns can be explored. It can also be used to simulate real-world infant skull injury cases given the impact conditions and material properties to predict if skull fracture will occur for a case and if so, what kinds of fracture can be expected. This can ultimately be used in the criminal justice system to assess — from a fundamental mechanics-based approach — the cause of observed fracture in human infant skulls.

5 Conclusion

This work presents the development, implementation and validation of a finite-element-based framework for simulating high-fidelity crack propagation during impact loading scenarios. The framework utilizes an adaptive remeshing technique to create a geometrically explicit representation of the crack. Stress intensity factors are calculated as crack-growth driving force to determine onset of crack propagation. Kink angles are calculated following principles of linear elastic fracture mechanics. Fracture-toughness anisotropy of human infant skull is modeled by considering its dependence on direction and crack length. Crack stability is also checked each time a crack propagates.

Three proof-of-concept simulations are presented to demonstrate the capability of the current framework. When compared to experiments, the simulated result predicts similar crack lengths and nominal crack-extension directions, which provide confidence in the capability of the modeling framework. However, the fracture parameters used in the model needs to be calibrated with experimental data once it become available. This framework is readily applicable to the study of other loading conditions, which makes it a suitable tool to study the influence of different impact scenarios on the resulting crack patterns, which could help to augment the limited number of experimental observations.

Acknowledgements This project was supported by Award No. 2016-DN-BX-0160, awarded by the National Institute of Justice, Office of Justice Programs, U.S. Department of Justice. The opinions, findings, and conclusions or recommendations expressed in this publication, program, exhibition are those of the authors and do not necessarily reflect those of the Department of Justice. Initial development of the infant skull model was supported by the Centers for Disease Control and Prevention grant NCIPC R49CE000411. The authors gratefully acknowl-

edge Dr. Bruce Carter for his technical support on issues regarding the use of FRANC3D.

Conflict of interest

The authors declare that they have no conflict of interest.

References

Asgharpour Z, Baumgartner D, Willinger R, Graw M, Peldschus S (2014) The validation and application of a finite element human head model for frontal skull fracture analysis. Journal of the mechanical behavior of biomedical materials 33:16–23

Bojtár I, Gálos M, Scharle A (1994) Fracture mechanical analysis of human skull. Periodica Polytechnica Civil Engineering 38(4):367–374

Chin PL (2011) Stress analysis, crack propagation and stress intensity factor computation of a ti-6al-4v aerospace bracket using ansys and franc3d. Sc Degree Rensselaer Polytechnic Institute Hartford Connecticut

Coats B (2007) Mechanics of head impact in infants. PhD thesis, University of Pennsylvania

Coats B, Margulies SS (2006) Material properties of human infant skull and suture at high rates. Journal of neurotrauma 23(8):1222–1232

Coats B, Ji S, Margulies SS (2007) Parametric study of head impact in the infant. Tech. rep., SAE Technical Paper

Corbani S, Castro J, Miranda A, Martha L, Carter B, Ingraffea A (2018) Crack shape evolution under bending-induced partial closure. Engineering Fracture Mechanics 188:493–508

Davis B, Wawrzynek P, Ingraffea A (2014) 3-d simulation of arbitrary crack growth using an energy-based formulation–part i: Planar growth. Engineering Fracture Mechanics 115:204–220

Erdogan F, Sih G (1963) On the crack extension in plates under plane loading and transverse shear. Journal of basic engineering 85(4):519–525

Farley R, Reece R, Robert M (2002) Recognizing when a childs injury or illness is caused by abuse. US Department of Justice, Office of Juvenile Justice and Delinquency Prevention, NCJ 160938

Fracture Analysis Consultants, Inc (2018) FRANC3D Reference Manual, Version 7.2. http://www.fracanalysis.com/software.html, online; accessed 16 February 2019

Got C, Patel A, Fayon A, Tarriere C, Walfisch G (1978) Results of experimental head impacts on cadavers: the various data obtained and their relations to some measured physical parameters. Tech. rep., SAE Technical Paper

Grassberger M, Gehl A, Püschel K, Turk E (2011) 3d reconstruction of emergency cranial computed tomography scans as a tool in clinical forensic radiology after survived blunt head traumareport of two cases. Forensic science international 207(1-3):e19–e23

Hajiaghamemar M, Lan IS, Christian CW, Coats B, Margulies SS (2018) Infant skull fracture risk for low height falls. International journal of legal medicine pp 1–16

Hazenberg JG, Taylor D, Lee TC (2006) Mechanisms of short crack growth at constant stress in bone. Biomaterials 27(9):2114–2122

Hodgson VR, Brinn J, Thomas L, Greenberg S (1970) Fracture behavior of the skull frontal bone against cylindrical surfaces. Tech. rep., SAE Technical Paper

Jacobsen C, Bech BH, Lynnerup N (2009) A comparative study of cranial, blunt trauma fractures as seen at medicolegal autopsy and by computed tomography. BMC medical imaging 9(1):18

Koester KJ, Ager Iii J, Ritchie R (2008) The true toughness of human cortical bone measured with realistically short cracks. Nature materials 7(8):672

Lee H, Choi J, Jung K, Im YT (2009) Application of element deletion method for numerical analyses of cracking. Journal of Achievements in Materials and Manufacturing Engineering 35(2):154–161

Leventhal JM, Thomas SA, Rosenfield NS, Markowitz RI (1993) Fractures in young children: distinguishing child abuse from unintentional injuries. American Journal of Diseases of Children 147(1):87–92

Li X, Sandler H, Kleiven S (2019) Infant skull fractures: Accident or abuse?: Evidences from biomechanical analysis using finite element head models. Forensic science international 294:173–182

Li Z, Luo X, Zhang J (2013) Development/global validation of a 6-month-old pediatric head finite element model and application in investigation of drop-induced infant head injury. Computer methods and programs in biomedicine 112(3):309–319

Li Z, Liu W, Zhang J, Hu J (2015) Prediction of skull fracture risk for children 0–9 months old through validated parametric finite element model and cadaver test reconstruction. International journal of legal medicine 129(5):1055–1066

Loyd AM (2011) Studies of the human head from neonate to adult: an inertial, geometrical and structural analysis with comparisons to the atd head. Duke University

Lynn PP, Ingraffea AR (1978) Transition elements to be used with quarter-point crack-tip elements. International Journal for Numerical Methods in Engineering 12(6):1031–1036

Metcalf RM, Comstock JM, Coats B (2019) High-rate anisotropic and region-dependent properties in human infant cranial bone

Nalla R, Stölken J, Kinney J, Ritchie R (2005) Fracture in human cortical bone: local fracture criteria and toughening mechanisms. Journal of biomechanics 38(7):1517–1525

Nguyen O, Repetto E, Ortiz M, Radovitzky R (2001) A cohesive model of fatigue crack growth. International Journal of Fracture 110(4):351–369

Pettit R, Annigeri B, Owen W, Wawrzynek P (2013) Next generation 3d mixed mode fracture propagation theory including hcf–lcf interaction. Engineering Fracture Mechanics 102:1–14

Pettit RG (2000) Crack turning in integrally stiffened aircraft structures

Raul JS, Baumgartner D, Willinger R, Ludes B (2006) Finite element modelling of human head injuries caused by a fall. International Journal of Legal Medicine 120(4):212–218

Roth S, Raul JS, Willinger R (2008) Biofidelic child head fe model to simulate real world trauma. Computer methods and programs in biomedicine 90(3):262–274

Roth S, Raul JS, Willinger R (2010) Finite element modelling of paediatric head impact: global validation against experimental data. Computer methods and programs in biomedicine 99(1):25–33

Sahoo D, Deck C, Yoganandan N, Willinger R (2013) Anisotropic composite human skull model and skull fracture validation against temporo-parietal skull fracture. Journal of the mechanical behavior of biomedical materials 28:340–353

Shih C, Lorenzi Hd, German M (1976) Crack extension modeling with singular quadratic isoparametric elements. International Journal of Fracture 12(4):647–651

Song JH, Areias PM, Belytschko T (2006) A method for dynamic crack and shear band propagation with phantom nodes. International Journal for Numerical Methods in Engineering 67(6):868–893

Spear AD, Priest AR, Veilleux MG, Ingraffea AR, Hochhalter JD (2011) Surrogate modeling of high-fidelity fracture simulations for real-time residual strength predictions. AIAA journal 49(12):2770–2782

US Department of Health & Human Services, Administration for Children and Families, Administration on Children, Youth and Families, Childrens Bureau (2019) Child maltreatment 2017.

https://www.acf.hhs.gov/cb/research-data-technology/statistics-research/child-maltreatment, online; accessed 8 August 2019

Vannier MW, Marsh JL, Warren JO (1984) Three dimensional ct reconstruction images for craniofacial surgical planning and evaluation. Radiology 150(1):179–184

Warzynek P, Carter B, Banks-Sills L (2005) The m-integral for computing stress intensity factors in generally anisotropic materials

Wawrzynek P, Carter B, Hwang CY, Ingraffea A (2010) Advances in simulation of arbitrary 3d crack growth using franc3dv5. Journal of the Computational Structural Engineering Institute of Korea 23(6):607–613

Weber W (1984) Experimental studies of skull fractures in infants. Zeitschrift fur Rechtsmedizin Journal of legal medicine 92(2):87–94

Weber W (1985) Biomechanical fragility of the infant skull. Zeitschrift fur Rechtsmedizin Journal of legal medicine 94(2):93–101

Yau J, Wang S, Corten H (1980) A mixed-mode crack analysis of isotropic solids using conservation laws of elasticity. Journal of applied mechanics 47(2):335–341

Zhang L, Yang KH, Dwarampudi R, Omori K, Li T, Chang K, Hardy WN, Khalil TB, King AI (2001) Recent advances in brain injury research: a new human head model development and validation. Tech. rep., SAE Technical Paper

Zimmermann EA, Launey ME, Ritchie RO (2010) The significance of crack-resistance curves to the mixed-mode fracture toughness of human cortical bone. Biomaterials 31(20):5297–5305